

A Comparative Study of EMG- and IMU-based Gesture Recognition at the Wrist and Forearm

Soroush Baghernezhad, *Student Member, IEEE*, Elaheh Mohammadreza, *Student Member, IEEE*, Vinicius Prado da Fonseca, *Member, IEEE*, Ting Zou, *Senior Member, IEEE*, and Xianta Jiang, *Senior Member, IEEE*

Abstract—Gestures are an integral part of our daily interactions with the environment. Hand gesture recognition (HGR) is the process of interpreting human intent through various input modalities, such as visual data (images and videos) and bio-signals. Bio-signals are widely used in HGR due to their ability to be captured non-invasively via sensors placed on the arm. Among these, surface electromyography (sEMG), which measures the electrical activity of muscles, is the most extensively studied modality. However, less-explored alternatives such as inertial measurement units (IMUs) can provide complementary information on subtle muscle movements, which makes them valuable for gesture recognition. In this study, we investigate the potential of using IMU signals from different muscle groups to capture user intent. Our results demonstrate that IMU signals contain sufficient information to serve as the sole input sensor for static gesture recognition. Moreover, we compare different muscle groups and check the quality of pattern recognition on individual muscle groups. We further found that tendon-induced micro-movement captured by IMUs is a major contributor to static gesture recognition. We believe that leveraging muscle micro-movement information can enhance the usability of prosthetic arms for amputees. This approach also offers new possibilities for hand gesture recognition in fields such as robotics, teleoperation, sign language interpretation, and beyond.

Index Terms—Inertial Measurement Unit (IMU), Electromyography (EMG), Hand Gesture Recognition (HGR), Prosthetic Control, Human-Computer Interaction (HCI)

I. INTRODUCTION

HAND gestures are intentional motions of the hands and fingers that play an important role in human interactions [1], from expressing an emotion to conveying a meaning. Hand gestures are also a great means of human and computer interaction (HCI) and have been used in a wide range of

This work has been submitted to the IEEE for possible publication. Copyright may be transferred without notice, after which this version may no longer be accessible.

Submitted on October 28th, 2025. This work was supported in part by the Government of Canada's New Frontiers in Research Fund (NFRF, Grant No NFRFE-2022-00407) and Natural Sciences and Engineering Research Council of Canada's Research Tools and Instruments (NSERC RTI, Grant No RTI-2022-00688).

This work involved human subjects or animals in its research. Approval of all ethical and experimental procedures and protocols was granted by the Memorial University Interdisciplinary Committee on Ethics in Human Research (20210316-SC).

Soroush Baghernezhad, Elaheh Mohammadreza, Vinicius Prado da Fonseca, and Xianta Jiang are with the Department of Computer Science, Memorial University of Newfoundland, St. John's, NL A1B 3X5, Canada. (email: sbagherneza@mun.ca, emohammadrez@mun.ca, vpradodafons@mun.ca, xiantaj@mun.ca).

Ting Zou is with the Department of Mechanical and Mechatronics Engineering, Memorial University of Newfoundland, St. John's, NL A1B 3X5, Canada. (email: tzou@mun.ca).

applications, including text input systems [2], air gesture control [3], prosthetic control [4], sign language recognition [5], rehabilitation [6], [7] etc. The formation of hand gestures

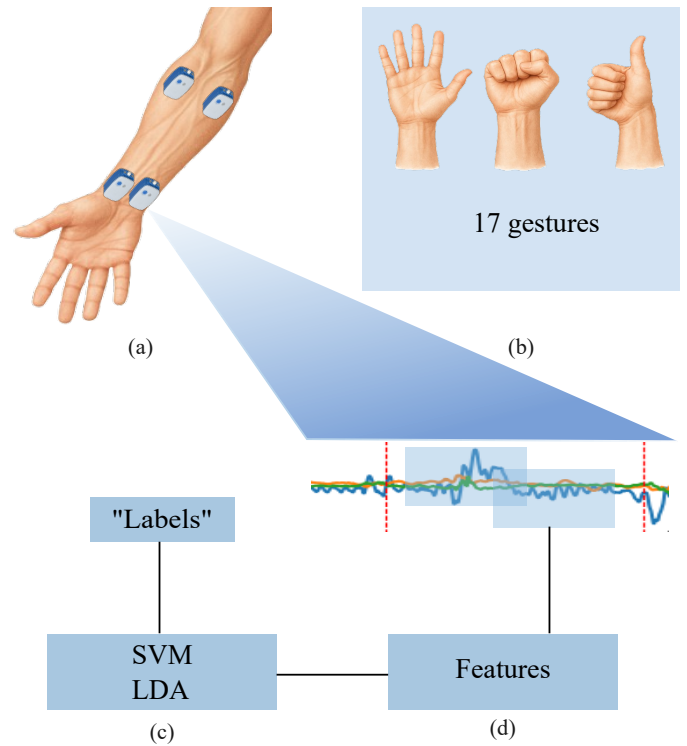


Fig. 1. Overview of our work. (a) Sensor Placement (b) Gestures (c) Feature Extraction (d) Model Training

begins in the brain, where signals are generated to control movements. These signals travel through the nervous system to the muscles in the arm and wrist, activating them to contract. This contraction results in tendon movements, skin and blood vessel deformation, and ultimately, hand gestures. These changes can be captured and used as input for pattern recognition systems [5].

Researchers have used wearable-sensor and vision-based approaches to acquire inputs for gesture recognition algorithms. Vision-based gesture recognition (VGR) approaches face several challenges, such as complex backgrounds that hinder hand segmentation, variations in illumination, hand movement, and occlusion of the hand gestures [8]. On the other hand, sensor-based approaches have been studied extensively, particularly

electrical sensors such as sEMG, which is the most commonly used modality in the literature [5]. However, sEMG signals are ineffective for detecting tendon movements [9]. Furthermore, the performance of sEMG-based systems is highly dependent on the placement of sensors on the arm or forearm, yet only a few studies have focused on optimizing sensor placement [10]–[12]. Inertial sensors, on the other hand, have been mostly used for human activity and gait detection, and not for static gesture recognition. A few studies have used IMU gloves for HGR [13], [14]; however, these gloves have several drawbacks, including the need for calibration and adjustment for different hand sizes and more importantly, they are not usable for amputees. Although IMUs have been used in combination with EMG [3], [15] for HGR, the potential of using inertial sensors alone, as well as their optimal placement, remains unexplored.

The goal of this study is to compare the performance of EMG and IMU sensors across different placements on the arm. To achieve this, eight EMG and IMU sensors were placed on different muscle groups to identify the optimal sensor locations. Each sensor recorded surface electromyography, accelerometer, gyroscope, and magnetometer data. The signals were then preprocessed and classified using various machine learning classifiers. Figure 1 provides an overview of our work.

Our main contributions are as follows:

- Leveraging tendon movements as supplementary information that cannot be captured by other commonly used sensors.
- Utilizing only IMU signals for static gesture classification.
- Identifying the optimal placement of IMU sensors on the arm to enhance classification performance.

The remainder of this paper is organized as follows. Section II reviews existing studies on hand gesture recognition, highlighting the advantages and limitations of various approaches. Section III details our proposed methodology, including data collection, preprocessing and signal evaluation, feature extraction, and classification. Section IV presents the experimental results, followed by a discussion where we analyze the findings and their implications. Section V concludes the paper and highlights the main findings. Finally, Section VI outlines potential directions for future research.

II. LITERATURE REVIEW

Video-based HGR methods use RGB, depth, or infrared cameras to capture hand motion, relying on image sequences and computer vision algorithms [16]. Optical tracking systems typically use cameras along with reflective markers placed on the body. These systems track marker positions in 3D space and are often used in biomechanics and motion capture [8]. For classification, researchers begin with preprocessing the raw data, followed by detecting and segmenting the gesturing part of the hand in images or videos. The gestures are then represented using a feature space, from which useful features are extracted. Finally, the extracted features are fed into classification algorithms to train models and predict the correct gestures [8].

In wearable-sensor approaches, one or more sensors are placed on the wrist [3], [10], arm [10], back of the hand, or

fingers [17]. These sensors can be electrical, such as EMG [18] and electrical impedance tomography (EIT); mechanical, such as force myography (FMG) [19], [20] and inertial measurement units (IMU); optical, such as photoplethysmography (PPG); or acoustical, such as mechanomyography (MMG) [4].

In previous studies, researchers have utilized different input modalities for pattern recognition, with sEMG being the most commonly used sensor in the literature. The authors in [10] used sEMG sensors and demonstrated that wrist signals are effective for both single- and multi-gesture recognition, achieving an average accuracy of 84.5% on 17 gestures with a selected set of features. In this study, they exclusively used sEMG sensors and collected data from a fixed arm position. The authors in [21] used three sEMG sensors on the forearm and achieved an accuracy of 94% using an artificial neural network (ANN) on 10 gestures. However, their accuracy decreased when the number of gestures increased. The authors in [22] used an RNN with GRU cells to predict 20 hand gestures in real time, achieving an accuracy of 89.6% using a 200 ms window of data. Combination of different deep learning methods has also been explored. The authors in [23] leveraged a CRNN, which combines both CNN and RNN models, to train a universal model capable of performing well on subjects that were not included in the training data.

IMUs have also been used in the literature for HGR, Motion and gait analysis [24]. The authors in [25] used 16 IMUs on a data glove to measure the range of motion in rheumatoid arthritis patients. In [13], the authors implemented five IMUs on the fingertips of a data glove. They used a random forest (RF) classifier to classify 26 gestures in French Sign Language, achieving an overall accuracy of 92.4%. The authors in [14] also used a data glove with three IMU sensors mounted on the index, thumb, and middle fingers and employed an LSTM combined with an ANN to classify 11 gestures. Kefer et al. [26] evaluated whether IMU data from the wrist could outperform data from the forearm for dynamic gesture classification. However, they found no significant difference between the classification accuracies of IMUs placed on the wrist and forearm.

Sensor fusion is another technique that has been used to improve the accuracy of classifiers. The authors in [15] used sensor fusion techniques to leverage both EMG and IMU data for training user-independent models to classify seven different gestures. They achieved a mean accuracy of 84.6% when using both EMG and IMU. Jiang et al. [3] fused both IMU and sEMG data to classify eight air and surface gestures using linear discriminant analysis (LDA). They achieved an accuracy of 92.8% and suggested that wrist-worn bands are helpful for real-time gesture recognition. However, the feasibility of IMU-only wristband devices was not studied in their work.

Some studies investigate the optimal placement of sensors. In [27], the authors addressed the challenge of finding a stable sensor placement on the hand while preserving informative signals. They reduced the number of sEMG electrodes from 30 to only 7. The authors in [11] also used sEMG to evaluate optimal placement of sensors for prosthetic control and suggested that placing two sensors on the wrist yields the best accuracy. Authors in [12] investigated the placement of IMU

TABLE I
COMPARISON OF SENSOR-BASED HGR STUDIES

Work	Sensor	Placement	Muscles	Type of gestures	Number of gestures	Number of participants	Method	Accuracy
Botros et al. [10]	sEMG	wrist and forearm	FCU, ED, ECU, EDM, BRR, FCR, PL, FDS	static	17	21	LDA-SVM	84.5
Lee et al. [21]	sEMG	forearm	FCU, FCR, BR	static	10	10	ANN	94
Zhang et al. [22]	sEMG	forearm	-	static	20	13	RNN	89.6
Kim et al. [23]	sEMG	forearm	-	dynamic	10	7	CRNN	96.04
Mummadi et al. [13]	IMU	hand	-	static	22	57	RF	92.4
Lauss et al. [14]	IMU	hand	-	-	11	22	LSTM + ANN	93
Kefer et al. [26]	IMU	wrist and forearm	-	dynamic	8	8	KNN, RF, DT	83.52 to 94.44
Alfaro et al. [15]	sEMG, IMU	forearm	ECU	static	7	22	Adaptive LS-SVM	92.4
Jiang et al. [3]	sEMG, IMU	wrist	FDS, BR, FCU, ED	air and surface	8	10	LDA	92.8

sensors for assessing upper limb motion and suggested the optimal positions for placing inertial sensors on the forearm, upper arm, and scapula. Studies related to gesture classification are summarized in table I.

III. METHODOLOGY

A. Sensor Placement

For this study, Noraxon Ultium system is used to capture sEMG and IMU data. Each sensor unit contains both sEMG and IMU sensors, and 8 units were used in this study. sEMG signals are recorded at 2000 Hz, and IMU is recorded at 200 Hz. Noraxon MR3 software was employed for data collection.

As suggested by [28], we placed our sensors parallel to the muscle fibers. The muscle groups were selected to ensure that the primary muscles responsible for the desired hand gestures were targeted [29]. Four sensor units (sEMG + IMU) are being placed circumferentially around the wrist (W1-W4), and the other four were placed circumferentially around the forearm (F1-F4) as shown in Figure 2. Our sensor placements are as follows (for the left arm):

- F1: Positioned on the brachioradialis (BR), with the potential to capture motions of the deeper layers, including the pronator teres (PT) and extensor carpi radialis longus (ECRL).
- F2: Placed on the palmaris longus (PL) and flexor carpi radialis (FCR).
- F3: Positioned on the right side of the flexor digitorum profundus (FDP), flexor carpi ulnaris (FCU), and flexor digitorum superficialis (FDS) (opposite of F2), capturing signals from the deep layers.
- F4: Placed on the left side of the ulna, over the extensor digitorum (ED) and extensor carpi radialis brevis (ECRB) (opposite of F1), with remote capture of the ECRL and extensor carpi ulnaris (ECU).
- W1: Positioned over the flexor pollicis longus (FPL), part of the pronator quadratus (PQ), and the FCR tendon.
- W2: Placed over the PL tendon, flexor digitorum superficialis (FDS) muscle, and tendons, with the ability to also capture signals from the FDP.
- W3: On ECU and ED tendons.
- W4: On EPL, ECRB, and EPB tendons.

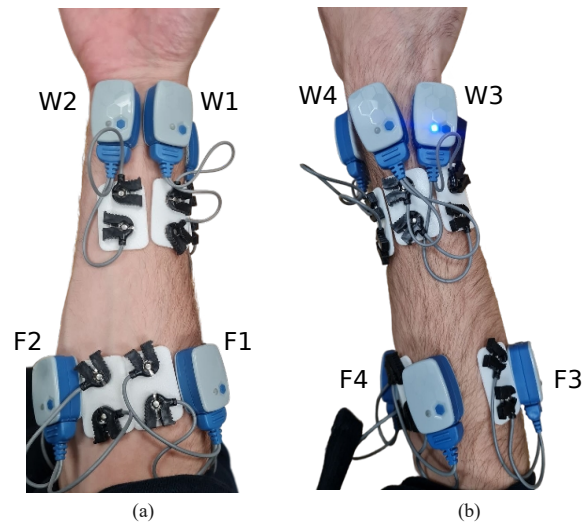


Fig. 2. Placement of sensors on (a) Anterior and (b) Posterior side of the arm.

Before sensor placement, the participants' arms were cleaned with rubbing alcohol to improve skin impedance [28]. The forearm and wrist were then examined while performing simple gestures to identify the corresponding muscles. Once the target muscles were located, the muscle group locations were marked using a cosmetic-grade, skin-safe marker. Subsequently, sensors were carefully placed on the marked locations.

B. Data Collection

For this study, data were collected from 12 able-bodied participants (age: 26 ± 3 years, 4 females, 8 males) with an average wrist circumference of 17.5 ± 2 cm, forearm circumference of 25.8 ± 3 cm, and forearm length of 25 ± 1.5 cm. All participants had no prior neuromuscular disorders. Prior to the experiment, they were given a consent form approved by Memorial University of Newfoundland Interdisciplinary Committee on Ethics in Human Research.

After securely placing the sensors on the participants' forearm and wrist, data collection was carried out in two phases. In phase one, participants were seated comfortably with their elbows bent at a 90-degree angle and their hands resting, as illustrated in Figure 3. In phase two, participants stood naturally with their arms positioned alongside their bodies. In both phases, visual instructions were displayed on a screen positioned in front of the participants. Before starting phase one, participants were asked to hold their hand in a stationary resting position for 15 seconds to collect the calibration data to be used in the signal analysis.

Prior to recording, participants were asked to practice the entire set of gestures once. During the experiment, they followed the visual instructions and performed 17 distinct gestures as shown in Figure 4. Each gesture was repeated four times, with each repetition lasting 2 seconds, followed by a 2-second rest period. Additionally, a 5-second rest was provided before the start of each new gesture to avoid muscle fatigue. After completing all 17 gestures, participants were allowed to rest before proceeding to the next position.

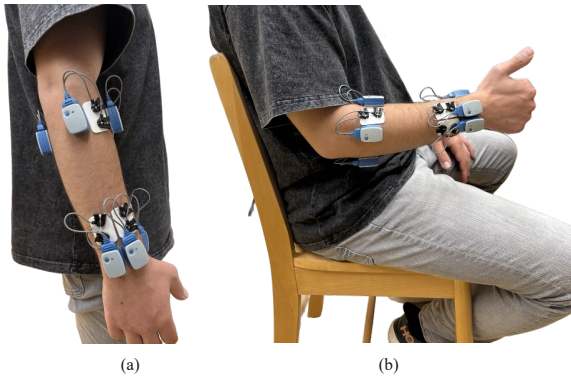


Fig. 3. (a) Participant postures during phase two and (b) phase one of the experiment.

The raw data were labeled using an automatic labeling method based on visual cues provided to the participants. Previous studies have shown that there is no significant difference in classification accuracy between automatic labeling and manual labeling based on video recordings of the experiment [30].

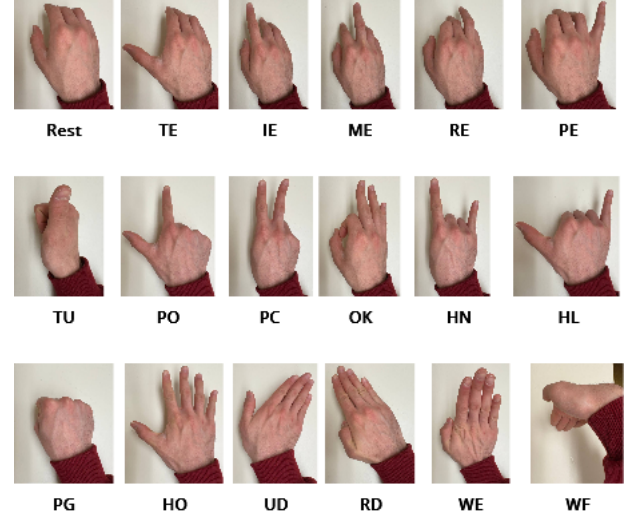


Fig. 4. Gestures used in this experiment. From top left: Rest, Thumb Extension (TE), Index Extension (IE), Middle Extension (ME), Ring Extension (RE), Pinky Extension (PE), Thumbs Up (TU), Pointing (PO), Peace (PC), OK, Horn (HN), Hang Loose (HL), Power Grasp (PG), Hand Open (HO), Ulnar Deviation (UD), Radial Deviation (RD), Wrist Extension (WE), and Wrist Flexion (WF).

EMG activation peaks were aligned with the corresponding labels.

C. Signal Quality Evaluation

For evaluating EMG and IMU signals, we use different metrics. For EMG signals, we first compute the calibration noise. To quantify baseline sensor noise during the calibration period, we computed the zero-mean standard deviation for each individual signal channel. For each signal $x = [x_1, x_2, \dots, x_N]$, where N is the number of samples collected during the calibration period, the mean μ was first removed to eliminate any DC offset, yielding a centered signal $x'_i = x_i - \mu$. The noise level was then defined as the standard deviation of the centered signal:

$$\sigma = \sqrt{\frac{1}{N} \sum_{i=1}^N (x'_i)^2} \quad (1)$$

For IMU data, which include tri-axial measurements from accelerometers, gyroscopes, and magnetometers, the zero-mean standard deviation was first calculated for each axis, and then averaged across axes to obtain a single noise value per sensor. These per-sensor noise levels were subsequently grouped by modality (EMG, accelerometer, gyroscope, magnetometer) and summarized using the mean and standard deviation across all sensors of the same type, providing a robust estimate of baseline noise for each modality. We also employed two metrics previously used in related studies [3], [10], with minor adjustments to tailor them to our current signals. These metrics are defined as follows:

- **Signal-to-Noise Ratio (SNR):** SNR compares the signal strength during the muscle activation phase to the noise level during the resting phase, where minimal or no signal amplitude is expected. Higher SNR values indicate

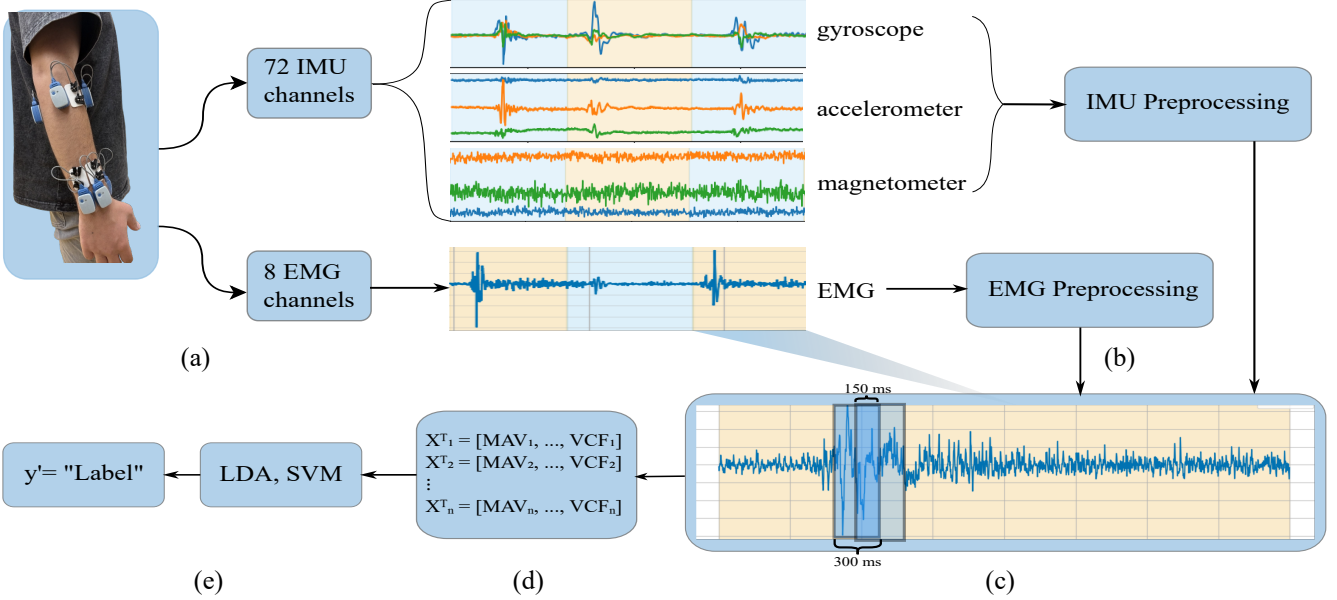


Fig. 5. Overview of the general pipeline used in this study. (a) Data collection (b) Filtering and preprocessing (c) Windowing (d) Feature extraction (e) Classification and Prediction

greater signal reliability. We used Eq. (2) to calculate the SNR for both EMG and IMU data. Note that the IMU signals were all zero-centered. After computing Eq. (2) for each channel, we averaged the results across all channels and then across all participants, respectively.

$$SNR = 20\log\left(\frac{RMS_{activation}}{RMS_{resting}}\right) \quad (2)$$

- **Signal to Motion Ratio (SMR):** SMR compares the power of the expected EMG signal with that of motion artifacts—unwanted noise generated by movement—and is calculated as follow:

$$SMR = 10\log_{10}\left(\frac{P_{EMG}}{P_{motion}}\right) \quad (3)$$

where

$$P_{EMG} = \sum_{f=0}^{500} PSD, \quad P_{motion} = \sum_{f=0}^{20} PSD \quad (4)$$

D. Preprocessing

We collect data at 2000 Hz for EMG and 200 Hz for IMU, which is then upsampled to 2000 Hz. Each gesture is repeated 4 times, yielding 16 seconds of data per gesture. Our dataset consists of a total of 10,880,000 samples per participant.

$$n_{samples} = (\text{duration}_{\text{gesture}} + \text{duration}_{\text{rest}}) \cdot n_{\text{repetitions}} \cdot n_{\text{gestures}} \cdot n_{\text{channels}} \cdot \text{frequency} \quad (5)$$

The raw EMG signals were first filtered using a notch filter to remove powerline noise. Subsequently, a band-pass filter between 20 Hz and 500 Hz was applied. The data were then smoothed using a window length of 50 and detrended to

eliminate baseline drift. Smoothing was also applied to the IMU signals.

A sliding window of 300 ms with a 150 ms overlap is used to segment the data, providing sufficient data while maintaining real-time performance [31]. After segmentation, a set of 22 time-domain and frequency-domain features is extracted from the EMG signals, while the same set of features, excluding MYOP and WAMP, is extracted from the IMU signals. These excluded features are threshold-based, and their thresholds were defined in previous EMG studies; therefore, they are not meaningful for IMU signals. Table II shows the list of extracted features. These features are among the most commonly used in the literature [3], [10], [32].

Since IMU signals are highly non-stationary and fluctuate rapidly, we require features that can quantify the overall signal energy and capture these fluctuations.

In this study, we use a modified set of time-domain features proposed in [10], which are designed to capture the signal attributes. We exclude features that are exclusively related to EMG by identifying those that rely on threshold-based computations.

E. Classification

To classify the gestures, we feed the features from the previous step into both Linear Discriminant Analysis (LDA) and Support Vector Machine (SVM) classifiers. We chose these two conventional machine learning models because they have been shown to be effective for gesture classification [3], [15], especially when compared to more advanced sequential models such as CRNN [23].

We use grid search for hyperparameter tuning, where `shrinkage` controls the regularization strength and `tol` sets the convergence tolerance in LDA, while in SVM, `C`

TABLE II
LIST OF EXTRACTED FEATURES [10]

Type	Feature Name	Abbreviation
Time Domain	Mean Absolute Value	MAV
	Variance	VAR
	Root Mean Square	RMS
	Waveform Length	WL
	Difference Absolute Mean Value	DAMV
	Difference Absolute STD	DASDV
	Zero Crossing	ZC
	Myopulse Percentage Rate	MYOP
	Willison Amplitude	WAMP
	Slope Sign Change	SSC
Frequency domain	Histogram, 10-bins	HIST
	AR Coefficients, 4 th Order	AR
	Mean Frequency	MNF
	Median Frequency	MDF
	Peak Frequency	PKF
	Total Power	TPP
	1 st Spectral Moment	SM1
	2 nd Spectral Moment	SM2
	3 rd Spectral Moment	SM3
	Frequency Ratio	FR
	Power Spectrum Ratio	PSR
	Variance of Central Frequency	VCF

regulates the trade-off between margin size and classification error, and the kernel type defines the mapping of data into higher-dimensional space. Model performance is evaluated using accuracy as the primary metric. We adopt a 4-fold stratified cross-validation strategy, where one repetition is held out as the test set in each fold. The final accuracy is computed by averaging the results across all folds. Figure 5 shows the overview of our pipeline.

F. Statistical analysis

This study aims to evaluate whether EMG signals provide a better performance compared to inertial sensing modalities over different sensor placements. We therefore defined four hypotheses: the first three address comparisons between EMG and each individual IMU component (accelerometer, gyroscope, and magnetometer), while the fourth assesses EMG relative to the combined contribution of all IMU components. These hypotheses are as follows:

$$H^{(1)} : \mu_{EMG} \geq \mu_{accel} \quad (6)$$

$$H^{(2)} : \mu_{EMG} \geq \mu_{gyro} \quad (7)$$

$$H^{(3)} : \mu_{EMG} \geq \mu_{mag} \quad (8)$$

$$H^{(4)} : \mu_{EMG} \geq \mu_{IMU_combined} \quad (9)$$

To assess the statistical significance and effect size between the two groups, we employed both hypothesis testing and effect size calculation. Normality of each group was first tested using the Lilliefors test [33]. If both distributions were found to be normal ($p > 0.05$), we used an independent two-sample t-test to compute the p-value. If at least one of the distributions deviated from normality, the Wilcoxon signed-rank test was applied instead. Additionally, Cohen's d was computed to quantify the effect size between the two groups, providing an interpretable measure of the magnitude

of difference regardless of statistical significance.

IV. RESULTS

A. Signal Evaluation results

As can be seen in Figure 6, most participants exhibit similar noise levels during the calibration phase for the EMG sensors, ranging from 3.30 to 7.07 μ V. The magnetometer also shows consistent noise levels across participants, ranging from 15.30 to 17.2 μ T, likely reflecting the stable background magnetic field. In contrast, the accelerometer and gyroscope readings vary considerably, with participants P06, P07, and P08 showing the highest deviations. This increased noise is likely due to small, unintended movements during the calibration phase.

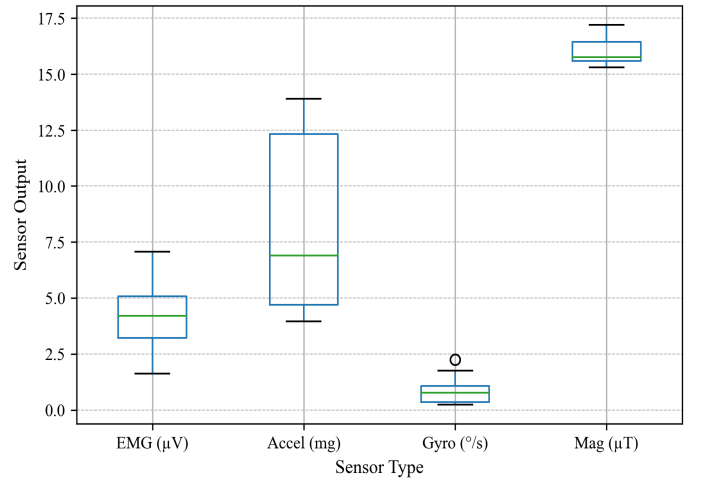


Fig. 6. Baseline noise levels (mean zero-mean standard deviation) during calibration for each participant.

In Table III, it can be observed that the signal strength of EMG relative to its noise is consistently higher than that of IMU, where noise is defined by Eq. (2). Additionally, wrist gestures tend to produce stronger EMG signals compared to single-finger gestures; however, this pattern does not hold for IMU signals. EMG also demonstrates higher SMR values than IMU. This difference can be attributed to the nature of IMU sensors, which can still detect subtle movements even in resting positions where muscles are not actively engaged.

B. Classification results

In Figure 7, the average accuracies of different sensors across various placements and postures are illustrated. It can be observed that using only acceleration sensor features consistently outperforms EMG features across all placements. SVM did not achieve satisfactory performance with EMG features overall. It is noteworthy that the random accuracy for 17 classes is approximately 5.9%. Both EMG and accelerometer sensor results exhibit high standard deviations, with EMG showing an average accuracy of $76 \pm 11\%$ and the accelerometer showing $84 \pm 8\%$, likely due to variations in participants' skin conditions, muscle mass, and contraction

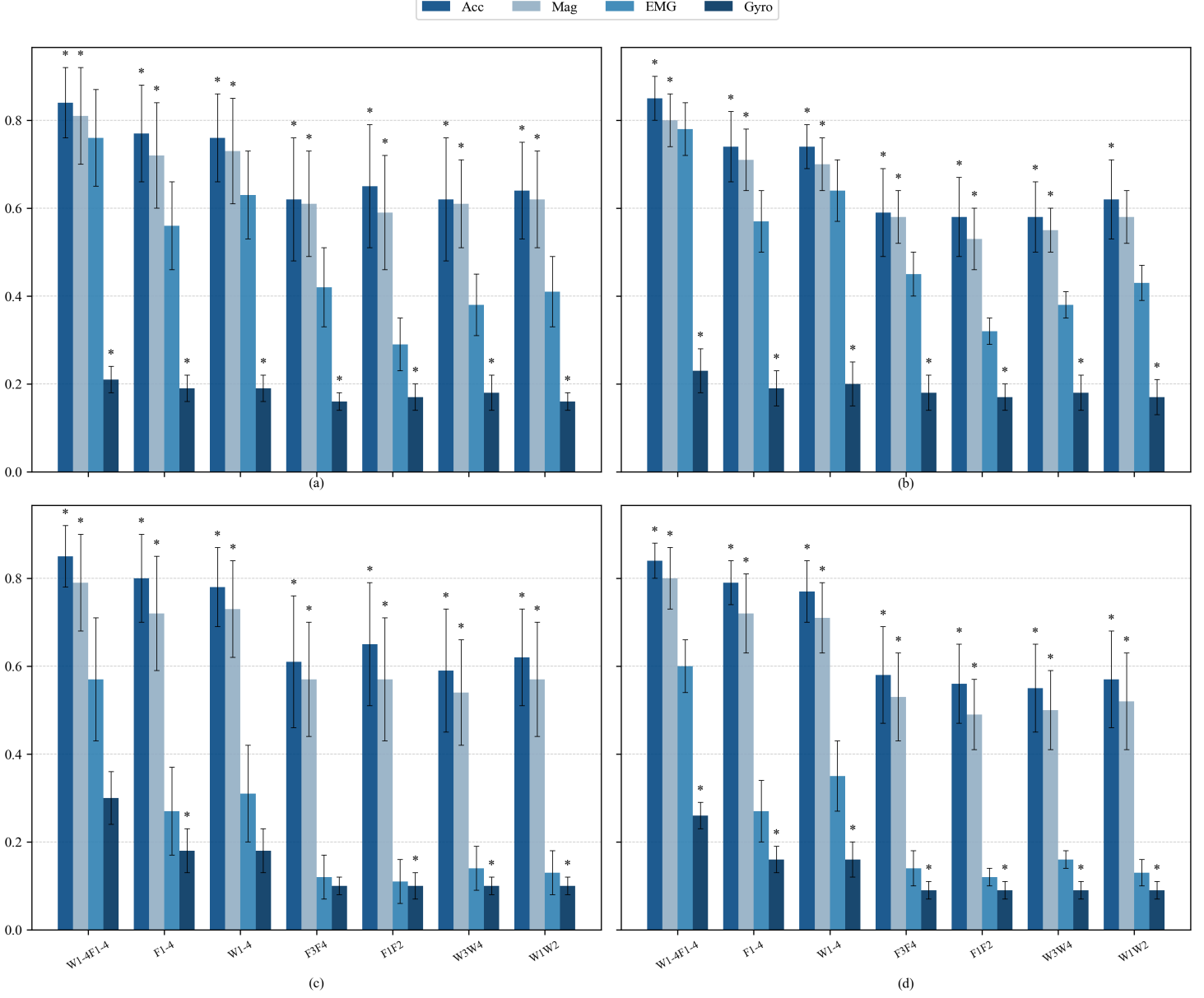


Fig. 7. Statistical Results for Classification accuracies EMG vs IMU sensors. (a) Comparison of EMG and IMU Sensors Using LDA Classifier at 90° Position, (b) LDA Classifier at 180° Position, (c) SVM Classifier at 90° Position, (d) SVM Classifier at 180° Position. Statistical significance is indicated by * ($p < 0.05$)

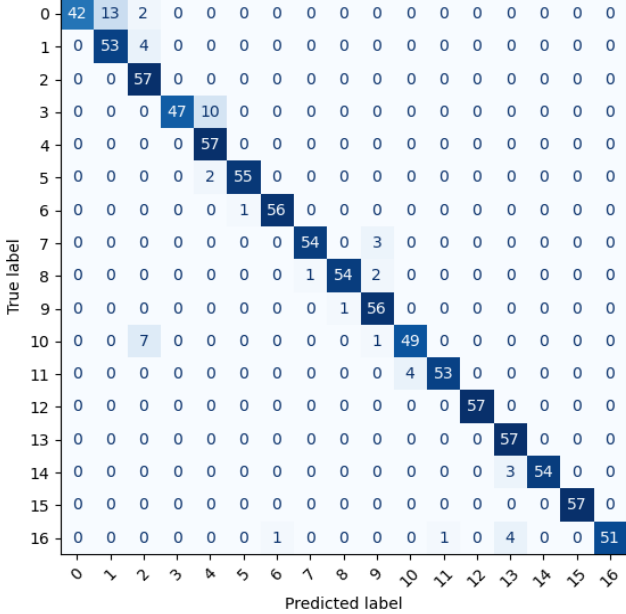
effort. Based on these results, the first hypothesis is rejected, as EMG did not outperform the accelerometer.

Changing the position of the arm from 90 degrees to 180 degrees does not substantially affect the trend in results, as shown in Figure 7 (b): in both 90-degree and 180-degree positions, acceleration sensor features consistently outperform EMG features across all placements. This suggests that acceleration-based features are robust to changes in arm position, maintaining superior classification accuracy regardless of posture.

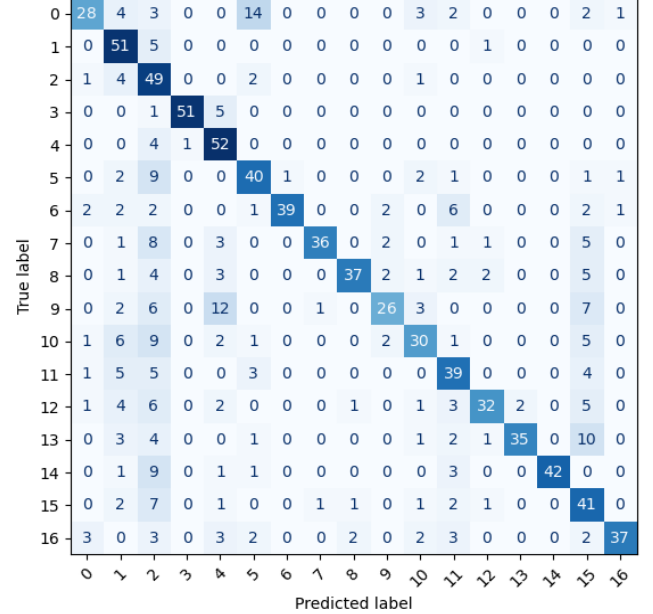
Gyroscope sensor, however, could not classify the gestures with high accuracy. As shown in Figure 7(a) and Figure 7(b), the EMG sensor consistently outperforms the gyroscope across all placements, which supports the second hypothesis. This

can be attributed to the gyroscope's sensitivity to rotational velocity, which is largely absent in static gestures.

We can also see that in all subfigures of Figure 7, magnetometer-based features outperform EMG features across all sensor placements and remain robust to changes in posture. Furthermore, the classification accuracies achieved by magnetometers are comparable to those of accelerometers, assuming no magnetic interference in the environment. The magnetometer captures the ambient magnetic field along multiple axes, and as the sensor moves, the recorded signals vary according to the direction of movement. These signal variations, even in response to subtle muscle movements, form meaningful patterns that can be effectively leveraged for static gesture classification. Therefore, our third hypothesis is rejected.



(a)



(b)

Fig. 8. Confusion matrix for all gestures of a single fold, from one participant. (a) IMU and (b) EMG . 0:TE 1:IE 2:ME 3:RE 4:PE 5:TU 6:RA 7:PO 8:OK 9:H 10:HL 11:PG 12:HO 13:WE 14:WF 15:UD 16:RD

#	SNR*			SMR*		
	EMG	IMU	<i>d</i>	EMG	IMU	<i>d</i>
0	5.10(1.66)	1.19(1.07)	2.80	35.78(5.90)	12.96(0.87)	5.41
1	3.01(1.50)	0.87(0.86)	1.75	33.21(7.24)	12.99(0.41)	3.94
2	4.09(1.87)	0.60(0.82)	2.41	35.31(8.46)	13.10(0.66)	3.70
3	5.33(2.32)	0.83(1.31)	2.38	34.88(7.24)	13.45(1.01)	4.15
4	3.88(1.70)	0.73(1.58)	1.93	33.95(6.00)	13.11(0.72)	4.87
5	4.56(2.12)	0.32(0.85)	2.63	32.28(6.45)	12.94(0.64)	4.22
6	5.79(1.31)	1.41(1.50)	3.12	37.27(7.32)	13.31(0.76)	4.60
7	3.91(1.41)	0.28(1.16)	2.81	32.78(7.41)	12.91(0.80)	3.77
8	5.30(2.50)	0.35(1.05)	2.58	33.78(6.80)	13.03(0.54)	4.30
9	5.06(1.87)	1.29(1.06)	2.49	32.87(7.61)	13.16(0.42)	3.66
10	5.59(1.88)	1.14(1.07)	2.92	34.42(6.36)	13.30(0.50)	4.68
11	4.16(2.35)	0.85(0.99)	1.83	33.02(7.10)	13.09(0.74)	3.95
12	6.22(2.30)	1.72(1.18)	2.47	34.45(3.94)	13.19(0.58)	7.55
13	6.98(2.85)	0.52(1.05)	3.00	33.61(5.57)	13.22(0.65)	5.15
14	6.96(2.87)	1.50(0.81)	2.58	33.00(4.93)	13.32(0.41)	5.62
15	6.51(3.58)	0.88(0.95)	2.15	33.95(4.47)	13.12(0.38)	6.57
16	5.79(2.59)	0.86(0.62)	2.62	32.62(7.49)	13.17(0.34)	3.67

TABLE III

DETAILED SNR AND SMR STATISTICS FOR EMG VS IMU ACROSS 17 GESTURES, 0:TE 1:IE 2:ME 3:RE 4:PE 5:TU 6:RA 7:PO 8:OK 9:H 10:HL 11:PG 12:HO 13:WE 14:WF 15:UD 16:RD, * INDICATES THAT ALL P-VALUES IN DIFFERENT GESTURES ARE BELOW 0.05.

Combining all features from the IMU sensors yields the highest classification performance, achieving an accuracy of $88.0 \pm 8.0\%$ when using data from all sensor placements in the 90° arm posture, and $89.0 \pm 3.0\%$ in the 180° arm posture. Detailed results for individual sensor placements are presented in Tables IV and V. The high effect sizes observed in both classifiers indicate a significant difference between the two groups. Additionally, we calculated the Davies–Bouldin Index (DBI), which measures clustering quality by evaluating the ratio of intra-cluster (within-cluster) dispersion to inter-cluster (between-cluster) separation; lower DBI values indicate better clustering performance. Based on these results, we reject our

fourth hypothesis as combined IMU components consistently outperform EMG. Figure 9 summarizes the classification results.

The confusion matrices of two models: LDA for IMU (left) and LDA for EMG (right) are shown in Figure 8. The performance of the EMG model decreases as the gestures become more complex, whereas the IMU model maintains consistent performance across different gestures. Moreover, the EMG model often confuses the TE gesture with TU, likely because both involve thumb extension, while TU additionally includes wrist rotation. In contrast, the IMU-based model appears more robust to such confusions.

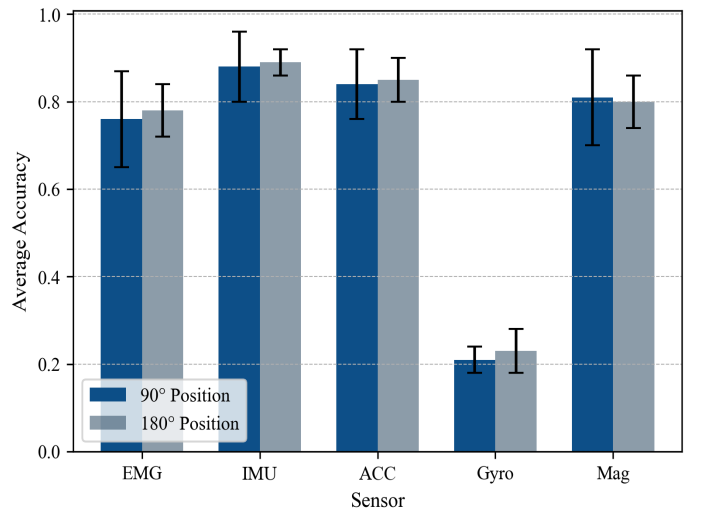


Fig. 9. Average accuracy of different sensor types on all placements.

TABLE IV

STATISTICAL RESULTS FOR CLASSIFICATION ACCURACIES EMG VS (ACCELEROMETER + GYROSCOPE + MAGNETOMETER) IN 90 DEGREE POSITION.

placement	LDA				SVM				DBI			
	EMG	IMU	p	d	EMG	IMU	p	d	EMG	IMU	p	d
W1W2	0.41(0.08)	0.74(0.10)	*	3.68	0.13(0.05)	0.74(0.09)	*	8.08	6.28(1.29)	2.43(0.98)	*	3.36
W3W4	0.38(0.07)	0.73(0.11)	*	3.66	0.14(0.05)	0.73(0.10)	*	7.33	4.66(1.84)	2.19(0.94)	*	1.69
F1F2	0.29(0.06)	0.76(0.11)	*	5.20	0.11(0.05)	0.76(0.10)	*	8.10	5.13(2.18)	2.12(1.03)	*	1.77
F3F4	0.42(0.09)	0.73(0.10)	*	3.24	0.12(0.05)	0.76(0.10)	*	7.82	5.30(1.71)	2.26(0.80)	*	2.28
W1-4	0.63(0.10)	0.83(0.09)	*	2.04	0.31(0.11)	0.82(0.08)	*	5.28	3.88(0.62)	2.23(0.97)	*	2.03
F1-4	0.56(0.10)	0.83(0.09)	*	2.83	0.25(0.10)	0.83(0.09)	*	6.21	4.40(1.24)	1.87(0.73)	*	2.48
W1-4F1-4	0.76(0.11)	0.88(0.08)	*	1.24	0.57(0.14)	0.87(0.07)	*	2.74	3.09(0.34)	2.02(0.99)	*	1.44

TABLE V

STATISTICAL RESULTS FOR CLASSIFICATION ACCURACIES EMG VS (ACCELEROMETER + GYROSCOPE + MAGNETOMETER) IN 180 DEGREE POSITION.

placement	LDA				SVM				DBI			
	EMG	IMU	p	d	EMG	IMU	p	d	EMG	IMU	p	d
W1W2	0.43(0.04)	0.73(0.06)	*	5.64	0.13(0.03)	0.75(0.08)	*	10.58	6.29(1.19)	1.99(0.81)	*	4.24
W3W4	0.38(0.03)	0.70(0.05)	*	7.11	0.16(0.02)	0.73(0.05)	*	14.10	6.19(1.47)	2.18(0.58)	*	3.58
F1F2	0.32(0.03)	0.69(0.09)	*	5.54	0.12(0.02)	0.73(0.10)	*	8.79	5.62(1.46)	2.35(0.81)	*	2.77
F3F4	0.45(0.05)	0.72(0.07)	*	4.43	0.14(0.04)	0.76(0.06)	*	11.48	5.89(0.65)	2.44(0.69)	*	5.14
W1-4	0.64(0.07)	0.83(0.05)	*	3.01	0.35(0.08)	0.83(0.04)	*	8.00	4.78(0.84)	2.04(0.77)	*	3.41
F1-4	0.57(0.07)	0.83(0.06)	*	3.93	0.27(0.07)	0.83(0.06)	*	8.48	4.91(1.06)	2.16(0.65)	*	3.13
W1-4F1-4	0.78(0.06)	0.89(0.03)	*	2.37	0.60(0.06)	0.87(0.04)	*	5.77	3.83(0.77)	2.09(0.86)	*	2.13

C. Optimal Placement

Our results indicate that sensor placement is a critical factor for achieving optimal classification performance with IMU sensors. When using only accelerometer data, placing sensors on either the anterior or posterior forearm, or on the wrist, yields comparable accuracies. However, the number of sensors and the extent of coverage across both anterior and posterior sides of the arm play a more significant role. As shown in Figure 7 configurations such as W1–W4 or F1–F4 result in higher accuracies compared to those covering only one side of the wrist (e.g., W1W2) or forearm.

This pattern is also observed when using magnetometer data. Furthermore, when incorporating all nine axes of the IMU (accelerometer, gyroscope, and magnetometer), results show that placing sensors on the anterior wrist yields better performance than the posterior wrist. Similarly, posterior forearm placements tend to outperform anterior forearm placements in certain models. Nevertheless, the general principle remains consistent: increasing the number of sensors to cover a broader range of muscle groups enhances classification accuracy. Specifically, deploying four sensors around the wrist or forearm improves accuracy by approximately 12%, while using eight sensors to cover both regions can lead to improvements of up to 20% compared to configurations with only two sensors on one side of the wrist.

V. CONCLUSION

The findings of this study highlight the potential of using IMU signals for static gesture classification, achieving an average accuracy of $89 \pm 3\%$. Our results indicate that while the anterior part of the wrist and the posterior part of the forearm

are more effective locations for IMU sensor placement, sensor quantity and coverage across different regions of the arm play an even more critical role in improving performance. Furthermore, although the wrist contains significantly less muscle mass than the forearm, making it challenging for surface EMG to capture high-quality signals, IMU sensors are capable of detecting subtle movements of muscles and tendons in the wrist area, providing valuable information for gesture recognition.

This work opens the door to more practical, robust, and non-invasive gesture recognition systems that do not rely on EMG, which is limited by susceptibility to noise, variability across sessions, and sensitivity to electrode positioning, or camera systems, enabling new possibilities in assistive technology and human-computer interaction.

VI. FUTURE WORK

This study demonstrated that IMU can serve as an alternative to EMG for static gesture recognition at the wrist and forearm, opening up several opportunities for future exploration. While this work focused on static gestures in controlled settings, extending it to dynamic gestures performed in more naturalistic environments is essential for practical applications. Evaluating robustness under conditions such as arm movement, sensor displacement, and long-term use will provide insights into the feasibility of IMU-based systems outside the laboratory. To further bridge the gap to daily real-world use, a promising direction is the development of an IMU-based wristband with embedded real-time gesture detection, designed for simplicity and reliability. Such a device could seamlessly connect to prosthetic hands or other electronics and

transmit control signals via BLE. Together, these directions represent important steps toward making IMU-based gesture recognition a practical and accessible solution for real-world human-machine interaction.

REFERENCES

- [1] T. Song, H. Zhao, Z. Liu, H. Liu, Y. Hu, and D. Sun, “Intelligent human hand gesture recognition by local-global fusing quality-aware features,” *Future Generation Computer Systems*, vol. 115, pp. 298–303, 2021. [Online]. Available: <https://www.sciencedirect.com/science/article/pii/S0167739X20318343>
- [2] J. Shin and C. M. Kim, “Non-Touch Character Input System Based on Hand Tapping Gestures Using Kinect Sensor,” *IEEE Access*, vol. 5, pp. 10496–10505, 2017.
- [3] S. Jiang, B. Lv, W. Guo, C. Zhang, H. Wang, X. Sheng, and P. B. Shull, “Feasibility of wrist-worn, real-time hand, and surface gesture recognition via semg and imu sensing,” *IEEE Transactions on Industrial Informatics*, vol. 14, no. 8, pp. 3376–3385, 2018. [Online]. Available: <https://ieeexplore.ieee.org/document/8141959/>
- [4] S. Jiang, P. Kang, X. Song, B. Lo, and P. Shull, “Emerging wearable interfaces and algorithms for hand gesture recognition: A survey,” *IEEE Reviews in Biomedical Engineering*, vol. 15, pp. 85–102, 2022. [Online]. Available: <https://ieeexplore.ieee.org/document/9426433/>
- [5] J. Shin, A. S. M. Miah, M. H. Kabir, M. A. Rahim, and A. Al Shiam, “A methodological and structural review of hand gesture recognition across diverse data modalities,” *IEEE Access*, vol. 12, pp. 142606–142639, 2024. [Online]. Available: <https://ieeexplore.ieee.org/document/10669579/>
- [6] J. Connolly, J. Condell, B. O’Flynn, J. T. Sanchez, and P. Gardiner, “Imu sensor-based electronic goniometric glove for clinical finger movement analysis,” *IEEE Sensors Journal*, pp. 1–1, 2018. [Online]. Available: <http://ieeexplore.ieee.org/document/8118157/>
- [7] L. Liu, X. Chen, Z. Lu, S. Cao, D. Wu, and X. Zhang, “Development of an EMG-ACC-based upper limb rehabilitation training system,” *IEEE Transactions on Neural Systems and Rehabilitation Engineering*, vol. 25, no. 3, pp. 244–253, 2016.
- [8] B. K. Chakraborty, D. Sarma, M. Bhuyan, and K. F. MacDorman, “Review of constraints on vision-based gesture recognition for human-computer interaction,” *IET Computer Vision*, vol. 12, no. 1, pp. 3–15, 2018. [Online]. Available: <https://ietresearch.onlinelibrary.wiley.com/doi/abs/10.1049/iet-cvi.2017.0052>
- [9] S. An, J. Feng, E. Song, K. Kong, J. Kim, and H. Choi, “High-Accuracy Hand Gesture Recognition on the Wrist Tendon Group Using Pneumatic Mechanomyography (pMMG),” *IEEE Transactions on Industrial Informatics*, vol. 20, no. 2, pp. 1550–1561, 2024.
- [10] F. S. Botros, A. Phinyomark, and E. J. Scheme, “Electromyography-based gesture recognition: Is it time to change focus from the forearm to the wrist?” *IEEE Transactions on Industrial Informatics*, vol. 18, no. 1, pp. 174–184, 2022. [Online]. Available: <https://ieeexplore.ieee.org/document/9275331/>
- [11] L. Chaplot, S. Houshmand, K. B. Martinez, J. Andersen, and H. Rouhani, “Optimizing Sensor Placement and Machine Learning Techniques for Accurate Hand Gesture Classification,” *Electronics*, vol. 13, no. 15, 2024. [Online]. Available: <https://www.mdpi.com/2079-9292/13/15/3072>
- [12] G. Höglund, H. Grip, and F. Öhberg, “The importance of inertial measurement unit placement in assessing upper limb motion,” *Medical Engineering & Physics*, vol. 92, pp. 1–9, 2021. [Online]. Available: <https://www.sciencedirect.com/science/article/pii/S1350453321000333>
- [13] C. K. Mummadi, F. P. P. Leo, K. D. Verma, S. Kasireddy, P. M. Scholl, J. Kempfle, and K. V. Laerhoven, “Real-Time and Embedded Detection of Hand Gestures with an IMU-Based Glove,” *Informatics*, vol. 5, no. 2, 2018. [Online]. Available: <https://www.mdpi.com/2227-9709/5/2/28>
- [14] D. Lauss, F. Eibensteiner, and P. Petz, “A Deep Learning based Hand Gesture Recognition on a Low-power Microcontroller using IMU Sensors,” in *2022 21st IEEE International Conference on Machine Learning and Applications (ICMLA)*, 2022, pp. 733–736.
- [15] J. G. Colli Alfaro and A. L. Trejos, “User-Independent Hand Gesture Recognition Classification Models Using Sensor Fusion,” *Sensors*, vol. 22, no. 4, 2022. [Online]. Available: <https://www.mdpi.com/1424-8220/22/4/1321>
- [16] A. S. Al-Shamayleh, R. Ahmad, M. A. M. Abushariah, K. A. Alam, and N. Jomhari, “A systematic literature review on vision based gesture recognition techniques,” *Multimedia tools and applications*, vol. 77, no. 21, pp. 28121–28184, 2018.
- [17] J. Connolly, J. Condell, B. O’Flynn, J. T. Sanchez, and P. Gardiner, “IMU Sensor-Based Electronic Goniometric Glove for Clinical Finger Movement Analysis,” *IEEE Sensors Journal*, vol. 18, no. 3, pp. 1273–1281, 2018.
- [18] X. Jiang, L.-K. Merhi, Z. G. Xiao, and C. Menon, “Exploration of Force Myography and surface Electromyography in hand gesture classification,” *Medical Engineering & Physics*, vol. 41, pp. 63–73, 2017. [Online]. Available: <https://www.sciencedirect.com/science/article/pii/S1350453317300176>
- [19] X. Jiang, L.-K. Merhi, and C. Menon, “Force Exertion Affects Grasp Classification Using Force Myography,” *IEEE Transactions on Human-Machine Systems*, vol. 48, no. 2, pp. 219–226, 2018.
- [20] A. Kadkhodayan, X. Jiang, and C. Menon, “Continuous Prediction of Finger Movements Using Force Myography,” *Journal of Medical and Biological Engineering*, vol. 36, 07 2016.
- [21] K. H. Lee, J. Min, and S. Byun, “Electromyogram-Based Classification of Hand and Finger Gestures Using Artificial Neural Networks,” *Sensors*, vol. 22, p. 225, 12 2021.
- [22] Z. Zhang, C. He, and K. Yang, “A Novel Surface Electromyographic Signal-Based Hand Gesture Prediction Using a Recurrent Neural Network,” *Sensors*, vol. 20, no. 14, 2020. [Online]. Available: <https://www.mdpi.com/1424-8220/20/14/3994>
- [23] E. Kim, J. Shin, Y. Kwon, and B. Park, “EMG-Based Dynamic Hand Gesture Recognition Using Edge AI for Human–Robot Interaction,” *Electronics*, vol. 12, no. 7, 2023. [Online]. Available: <https://www.mdpi.com/2079-9292/12/7/1541>
- [24] X. Jiang, C. Napier, B. Hannigan, J. J. Eng, and C. Menon, “Estimating Vertical Ground Reaction Force during Walking Using a Single Inertial Sensor,” *Sensors*, vol. 20, no. 15, 2020. [Online]. Available: <https://www.mdpi.com/1424-8220/20/15/4345>
- [25] J. Connolly, J. Condell, B. O’Flynn, J. Sanchez, and P. Gardiner, “IMU Sensor-Based Electronic Goniometric Glove for Clinical Finger Movement Analysis,” *IEEE Sensors Journal*, vol. 18, no. 3, pp. 1273–1281, Feb. 2018, publisher Copyright: © 2001–2012 IEEE.
- [26] K. Kefer, C. Holzmann, and R. D. Findling, “Evaluating the placement of arm-worn devices for recognizing variations of dynamic hand gestures,” *J. Mob. Multimedia*, vol. 12, no. 3–4, p. 225–242, Apr. 2017.
- [27] N. Jarque-Bou, M. Vergara, J. Sancho-Bru, A. Roda-Sales, and V. Gracia, “Identification of forearm skin zones with similar muscle activation patterns during activities of daily living,” *Journal of NeuroEngineering and Rehabilitation*, vol. 15, 10 2018.
- [28] P. Konrad, *ABC of EMG – A Practical Introduction to Kinesiological Electromyography*. Noraxon Inc. USA, 2006, version 1.4; March 2006, ISBN 0-9771622-1-4.
- [29] H. Frank and M. Netter, *Atlas of human anatomy*. Elsevier Inc., 2019.
- [30] E. Mohammadreza, V. P. Da Fonseca, and X. Jiang, “Investigating the Impact of Training Protocols on Myoelectric Pattern Recognition Control in Upper-Limb Amputees,” *IEEE Transactions on Neural Systems and Rehabilitation Engineering*, pp. 1–1, 2025.
- [31] B. Hudgins, P. Parker, and R. Scott, “A new strategy for multifunction myoelectric control,” *IEEE Transactions on Biomedical Engineering*, vol. 40, no. 1, pp. 82–94, 1993.
- [32] A. Phinyomark, F. Quaine, S. Charbonnier, C. Serviere, F. Tarpin-Bernard, and Y. Laurillau, “EMG feature evaluation for improving myoelectric pattern recognition robustness,” *Expert Systems with Applications*, vol. 40, no. 12, pp. 4832–4840, 2013. [Online]. Available: <https://www.sciencedirect.com/science/article/pii/S0957417413001395>
- [33] H. W. Lilliefors, “On the kolmogorov-smirnov test for normality with mean and variance unknown,” *Journal of the American Statistical Association*, vol. 62, no. 318, pp. 399–402, 1967. [Online]. Available: <http://www.jstor.org/stable/2283970>